

On the Electrochemical Reduction of 4-(Thiazol-2-ylazo)-Substituted 1-Chloronaphthalenes: Formation and Characterization of Stable Radical Anions

Evgenia Dmitrieva,^[a] Alexey A. Popov,^[a] Xiuling Yu,^[b] and Horst Hartmann^{*,[b]}

The electrochemical reduction of two chloro-substituted 4-(thiazol-2-ylazo) has been studied by means of spectroelectrochemistry and simulated with the DFT method. Whereas the 1-chloro-4-(4-chlorothiazol-2-ylazo) forms both a stable radical anion and a dianion, the dianion of 1-chloro-4-(thiazol-2-ylazo) is instable. In the radical anion of both compounds, the spin

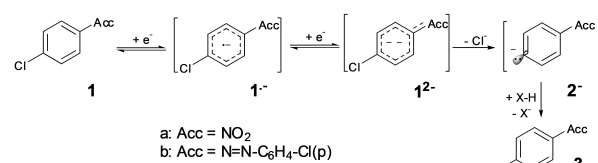
densities are high not only at the azo moiety but also at C3 in the naphthalene and at C5 in the thiazole moiety. This is in agreement with former experimental results demonstrating the remarkable reactivity of these positions towards thiols which can act as nucleophiles as well as electron donors.

1. Introduction

Radical anions derived from simple halogen-substituted aromatic compounds generated by a one-electron transfer are known to undergo a cleavage of the halogen-carbon bond with the loss of the halide ion.^[1] However, when the aromatic halide contains additional electron-withdrawing groups, such as a nitro group like in the compound **1a**, the radical anion **1a^{•-}** becomes less reactive so that it can be observed, e.g. by means of spectroelectrochemistry,^[2] and transformed at higher potentials into the corresponding dianion **1a²⁻** (Scheme 1). However, this dianion is rather instable and loses its halogen as chloride ion under formation of a σ -type mono-anion **2a⁻**, which usually accepts a proton from a suited proton donor XH, such as residual water, so that the reduced species **3a** results from **1a**.^[3]

A similar behavior was found also for halogen substituted azo benzenes. As exemplified for 4,4'-dichloro azobenzene **1b**, in aprotic solution this compound can be transformed electrochemically into a stable radical anion **1b^{•-}** as well as into a less stable dianion **1b²⁻**. This dianion can also lose its chloride ion yielding the corresponding σ -type mono-anion **2b⁻** which can accept as a strong base a proton yielding the 4-chloroazobenzene **3b**.^[4]

In contrast to the electrochemical studies at the halogen-substituted azobenzenes none such investigations exist in the



Scheme 1. Formation and consecutive reaction of radical anions and dianions of acceptor-substituted chlorobenzenes.

series of heterocyclic azo compounds, such as the chloro-substituted 2-thiazolylazo compounds of the general structure **4** hitherto. Only for hydroxy- and amino-substituted 2-thiazolylazo compounds electrochemical studies have been reported, but no elimination of the substituents from the radical anions formed was observed.^[5]

Because in course of the reaction of the chloro-substituted 2-thiazolylazo compounds **4** with thiols RSH in presence of an auxiliary base, such as triethylamine, nine different mercapto-substituted products **5a–5j** are formed (Scheme 2), we have postulated for their formation three different reaction routes, including the one with radical species as intermediates (Scheme 3, route 3).^[6]

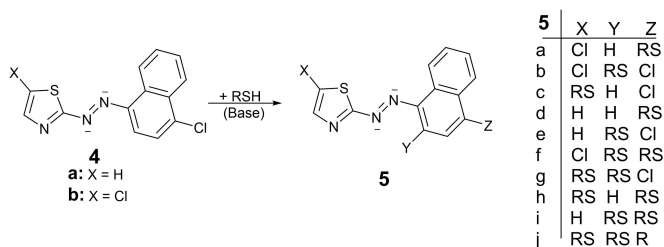
Thus, the first route consists in a usual nucleophilic substitution, which runs on a so-called Meisenheimer intermediate **A**. By chloride elimination from this intermediate the compound **5d** arises. The second route involves the formation

[a] Dr. E. Dmitrieva, Dr. A. A. Popov
Leibniz Institut für Festkörper- und Werkstofforschung (IFW)
Helmholtzstrasse 20, 1069, Dresden, Germany

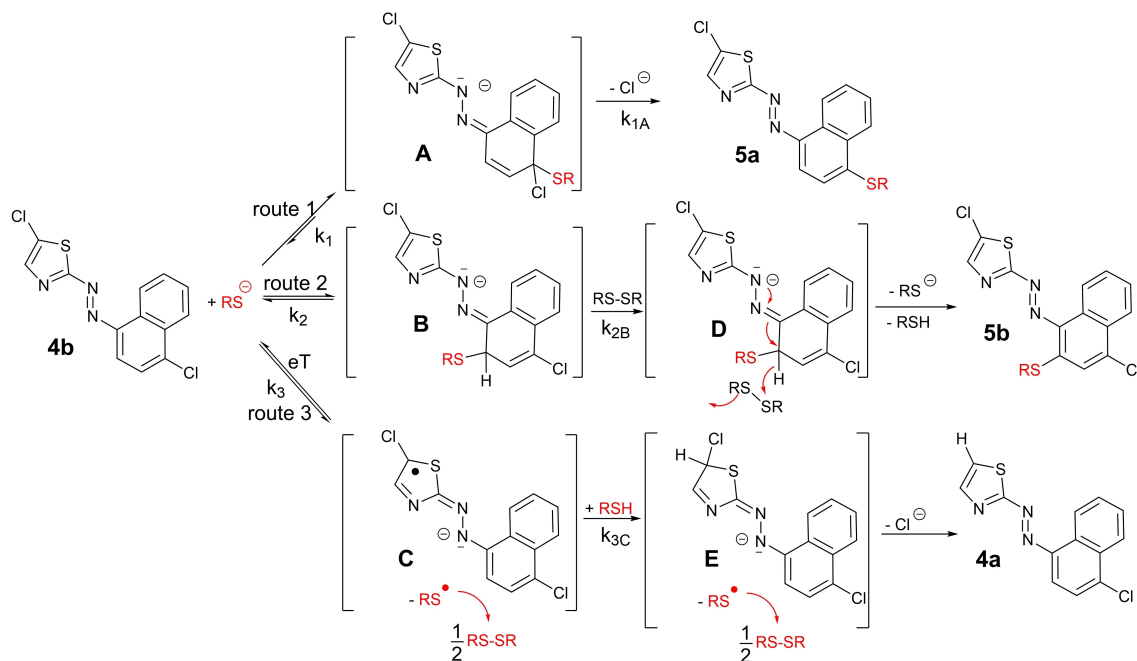
[b] Dr. X. Yu, Prof. Dr. H. Hartmann
Technische Universität Dresden,
Lehrstuhl Organische Chemie
Mommsenstrasse 6, 01062 Dresden, Germany
E-mail: horst.hartmann@tu-dresden.de

Supporting information for this article is available on the WWW under <https://doi.org/10.1002/celec.202000121>

© 2020 The Authors. Published by Wiley-VCH Verlag GmbH & Co. KGaA. This is an open access article under the terms of the Creative Commons Attribution License, which permits use, distribution and reproduction in any medium, provided the original work is properly cited.



Scheme 2. Products **5** of the reaction of 1-chloro-4-(thiazol-2-ylazo)**4** with thiols.



Scheme 3. Postulated mechanism of the reaction of the chloro-substituted thiazole azo compound **4b** with thiolates.

of a σ_{H} -complex **B** as intermediate formed by the addition of the nucleophilic thiol anion RS^- at an *H*-substituted naphthalene (or thiazole) moiety. Subsequently, this complex **B** transfers its σ -bonded *H*-atom as hydride ion on an electron acceptor, such as a disulfide which is present in the reaction mixture and was generated from the starting thiol, e.g. by air oxidation, yielding the compound **5e**.

Finally, the third route involves the intermediate formation of an azo radical anion **C** initiated by a single electron transfer from a thiol anion to the neutral azo compound **4b**. Subsequently, this radical anion **C** ($4\text{b}^{\cdot-}$) transfers an *H*-atom from a second thiol under formation of a Meisenheimer-type intermediate **E** from which a chloride ion is finally eliminated yielding the compound **4a**.

The last-mentioned reaction route in which the formation of an intermediate radical anion **C** was postulated stimulated us to study the electrochemical reduction of the chloro-substituted 2-thiazolyazo compounds **4a** and **4b** with the aim to indicate the formation of corresponding radical anions and to study their electronic and chemical properties.

2. Results and Discussion

The 1-halogen-substituted 4-(thiazol-2-ylazo) naphthalenes **4a** and **4b** used for this study were prepared by reaction of the known 4-thiazolyazo-substituted 1-naphthols^[7] with POCl_3 in presence of DMF according to a published procedure.^[6,8]

2.1. UV-Vis Absorption Spectroscopy

The UV-Vis absorption spectra of the compounds **4a** and **4b** measured in acetonitrile solution are presented in Figure 1. Both compounds exhibit absorption bands at 210 and 273 nm in the UV spectral region. The bands with the maxima at 413 nm and 435 nm (molar extinction coefficients $\approx 15,850 \text{ L mol}^{-1} \text{ cm}^{-1}$) are observed in the visible spectra of **4a** and **4b**, respectively. The optical energy gaps were calculated from the absorption maxima, which are 3.00 and 2.85 eV for **4a** and **4b**, respectively. Small variation of the excited state energies between **4a** and **4b** can be ascribed to the influence

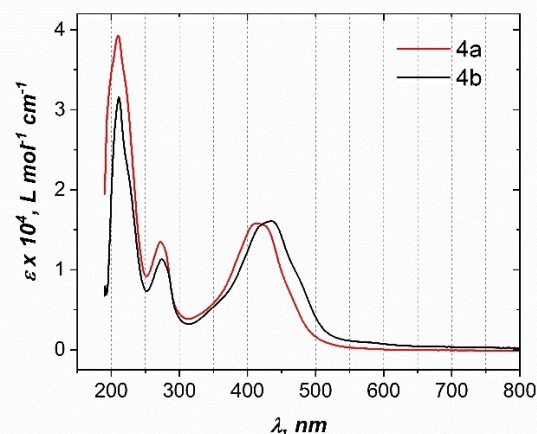


Figure 1. The UV-Vis absorption spectra of **4a** and **4b** in acetonitrile.

of Cl substituent in the thiazole moiety of **4b**, which lowers the LUMO energy (see below).

2.2. Electrochemical and Spectroelectrochemical Studies

To characterize the formation of reduced anionic species of **4a** and **4b** and to evaluate their stability in solution, both compounds were first studied by cyclic voltammetry (CV). As shown in Figure 2, the CV of compound **4a** exhibits two reversible one-electron reduction processes at half-wave potentials $E_1 = -1.17$ V and $E_2 = -1.95$ V (vs. Fc^+/Fc). The CV of compound **4b** measured with the sweep rate of 0.1 V/s shows a reversible one-electron reduction peak at half-wave potential $E_1 = -1.06$ V and irreversible reduction peaks at -1.85 and -1.95 V. At higher sweep rates, an additional reversible process with the half-wave potential of -1.17 V but with a lower peak current can be also detected for **4b** after several electrochemical cycles (see SI). The reversibility of the first reduction process of both compounds points to the high stability of the radical anions **4a $^{\bullet-}$** and **4b $^{\bullet-}$** generated at this step. Formation of the stable dianion **4a $^{2-}$** can be also concluded for the second reduction step of **4a**. At the same time, the dianion **4b $^{2-}$** is not stable as follows from the irreversible behaviour observed at the second reduction step of **4b**. Presumably, the dianion **4b $^{2-}$** eliminates the chloride ion from the thiazole moiety, leading to the formation of the compound **4a**. The processes at -1.17 and -1.95 V in the CV of **4b** can be then assigned to the reduction steps of **4a**.

The formation of radical anions of the compounds **4a** and **4b** during their first reduction processes was confirmed by ESR and UV-Vis-NIR spectroscopy. The changes of the spectral features for **4a** are shown in the Figure 3; analogous spectra of **4b** are deposited in SI.

Thus, during the first redox process of the compound **4a** the corresponding radical anion **4a $^{\bullet-}$** is generated which is characterized by an intense ESR signal with a g-value of 2.0042 and an absorption spectrum with an intense band at 542 nm and a less intense one at 780 nm. For the compound **4b**, the

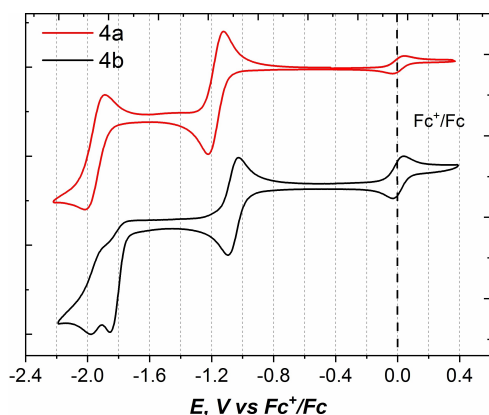


Figure 2. Cyclic voltammograms of 2-[(4-chloronaphthalen-1-yl)](**4a**) and 5-chloro-2-[(4-chloronaphthalen-1-yl)](**4b**) measured in acetonitrile (0.1 M $n\text{-Bu}_4\text{NPF}_6$) at the scan rate of 0.1 V/s.

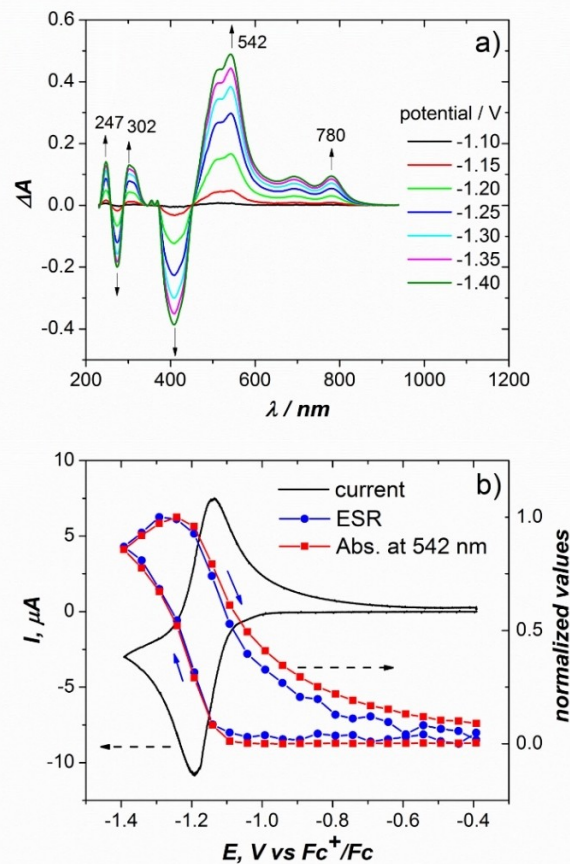


Figure 3. a) In situ UV-Vis-NIR spectra recorded during reduction of **4a**; b) dependence of the intensity of ESR signal and intense electronic absorption at 542 nm on the reduction potential.

generation of the radical anion **4b $^{\bullet-}$** during the first reduction is indicated by an intense ESR signal with a g-value of 2.0043 and an absorption spectrum with an intense maximum at 542 nm and a less intense band at 795 nm. The potential dependencies of the intensity of the ESR signal and absorption bands are in perfect agreement (Figure 3b). This observation allows the unambiguous assignment of these spectroscopic features to the radical anion species. The presence of two absorption bands at 542 nm and at about 790 nm found in the electronic absorption spectra of compounds **4a** and **4b** is in accordance with the absorption characteristics of radical anions derived from azobenzene or 4,4'-dichloroazobenzene, which exhibit in their absorption spectra two intense bands at about 400 and 460 nm as well as two low intense bands at about 605 and 620 nm, respectively.^[9]

When the potential sweep is extended to more negative values, the absorption bands of the radical anion decrease in the potential range from -1.8 to -2.2 V (Figure 4). The intensity of the ESR signal also decreases simultaneously (Figure 4, inset). On the reverse scan, both absorption and EPR features of the radical anion reappear again. It indicates that the radical anion **4a $^{\bullet-}$** is reversibly converted to the diamagnetic dianion **4a $^{2-}$** during the second reduction step.

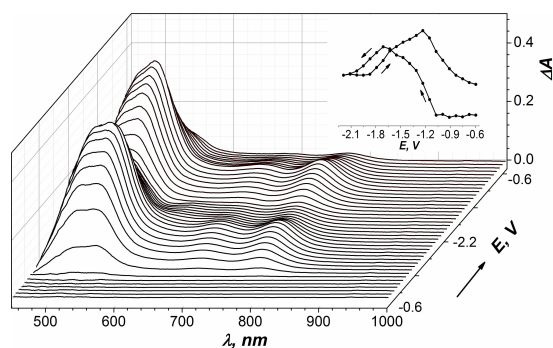


Figure 4. In situ Vis-NIR spectra recorded during the voltammetric cycle of **4a** (3D plot). Inset: Potential profile of the ESR intensity.

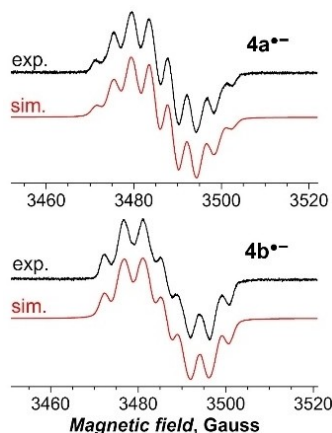


Figure 5. Experimental (black) and simulated (red) ESR spectra of **4a**^{•-} and **4b**^{•-}.

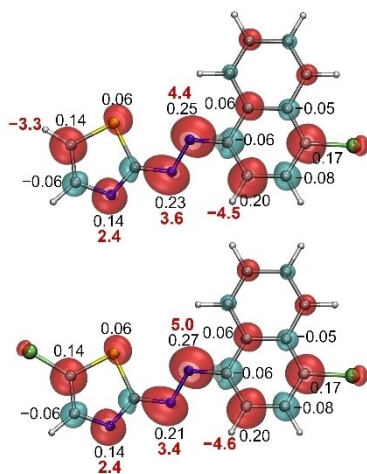


Figure 6. Spin density distribution in the radical anions **4a**^{•-} and **4b**^{•-} (red – positive, blue – negative). The numbers are hyperfine coupling constants (in Gauss, bold red) determined from the fit to the experimental ESR spectra (see Figure 5), and DFT-computed Mulliken spin populations (black).

2.3. Computational Studies of the Charged States

2.3.1. ESR Spectra of Radical Anions

Both anion radicals **4a**^{•-} and **4b**^{•-} exhibited hyperfine structure in their EPR spectra (Figure 5). For an interpretation of the spectra and description of the spin density distribution in the anions, DFT calculations have been performed. Spin density distribution in the radical anions are plotted in Figure 6. Both compounds show very similar distribution involving the whole molecule. The largest spin populations are predicted for the nitrogen atoms of the azo-bridge, at the C-atom in the 3-position of the naphthalene moiety and at the C-atom in the 5-position of the thiazole moiety. In contrast, chlorine atoms have rather low spin populations.

Computed hyperfine coupling (*hfc*) constants were then used as a first guess in fitting of the experimental ESR spectra.^[10] The procedure resulted in the perfect match between experiment and theory (Figure 5), and determined coupling constants are shown in Figure 6. In **4a**^{•-}, computations predict the largest *hfc* constants for three nitrogen atoms, one proton in the chloro-naphthalene moiety, and one proton in the five-membered thiazole ring. For other atoms, DFT predicts the constant in the range of 1 G or less, and the hyperfine structure due to these atoms cannot be resolved in the experimental spectra (the apparent line width is ca 2 G). In **4b**^{•-}, the chlorine substitutes the proton, which has large *hfc* constant in **4a**^{•-}, whereas the *hfc* constants of other atoms are not strongly affected by the substitution. As a result, the apparent octet in the spectrum of **4a**^{•-} turns to an apparent septet in **4b**^{•-} (Figure 5).

2.3.2. MO Structure and Absorption Spectra

Figure 7 show the Kohn-Sham molecular orbital levels in **4a**, **4a**^{•-}, and **4a**²⁻, whereas Figure 8 visualizes HOMO, and three lowest unoccupied orbitals of **4a**. Note that due to the different charge of the species, direct comparison of their orbital energies is not possible, but the relative energies are still reasonable.

For **4b**, calculations predict similar values except for the small shifts of the energies (see SI). In particular, the LUMO of **4b** is predicted to be 0.09 eV lower in energy than the LUMO of **4a**, whereas the HOMO energies of both compounds are virtually identical. The variation of the LUMO energy corresponds to the small difference in the reduction potentials and differences in the absorption maxima of **4a** and **4b**.

As can be seen in Figure 8, the HOMO of compound **4a** is delocalized over the whole molecule; the LUMO has higher contribution from the 5-membered ring and the azo-bridge, whereas LUMO+1 and LUMO+2 have predominant localization on the chloro-naphthalene moiety.

Excitation spectra were computed with time-dependent (TD) DFT using long-range corrected CAM-B3LYP functional (this is a modification of the B3LYP function with long-range correction). TD-DFT rarely gives very exact prediction of

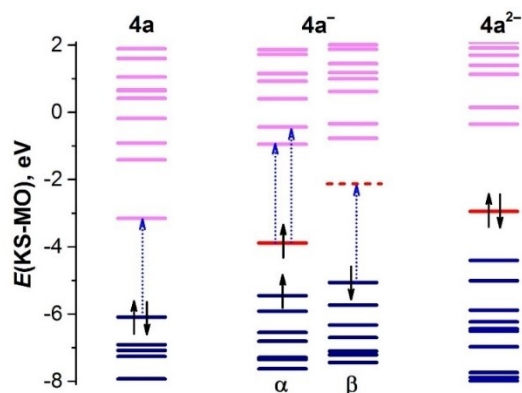


Figure 7. Energy levels of Kohn-Sham molecular orbitals (B3LYP/def2-TZVPP level, with C-PCM solvation correction for acetonitrile). Occupied levels are shown as dark blue lines, unoccupied – as light magenta. The levels of the anions originating from the LUMO of the neutral molecule are shown in red (singly-occupied MO in the anion and the HOMO of the dianion). For the radical anion, the energies of the spin-up (α) and spin-down (β) MOs are shown separately. Blue dotted arrows show main configurations in the transition with considerable intensity.

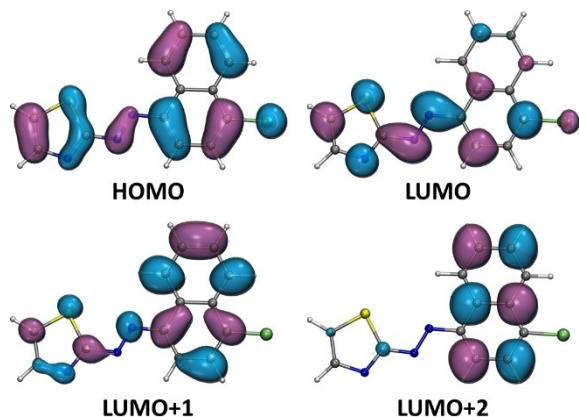


Figure 8. Isosurface of selected molecular orbitals of **4a**. **4b** has essentially the same orbital shape.

excitation energies, but general trends are usually predicted correctly. Excitation energies and intensities for in **4a** and **4a^{•-}** are shown in Figure 9 along with the isosurfaces of the electron density differences ($\Delta\rho$) for each excitation with considerable oscillator strength. If electron excitation is understood as a formation of an electron/hole pair, $\Delta\rho$ essentially visualizes its spatial distribution.

For the neutral molecule **4a**, TD-DFT predicts one intense transition in the visible range near 486 nm (Figure 9) which corresponds to the experimentally observed absorption band at 415 nm. In terms of molecular orbitals, this transition is described as a single configuration with predominant HOMO \rightarrow LUMO excitation. In terms of the difference density, one can see that the electron is transferred from the rings and is localized on the azo-bridge

In the radical anion **4a^{•-}**, the electron occupies the LUMO of the neutral molecule, which therefore turns into the singly occupied MO (SOMO). The SOMO level is considerably split. Furthermore, considerable polarization can be seen for the

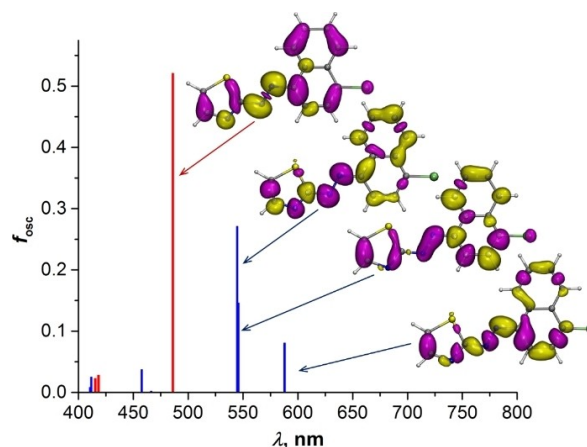


Figure 9. Low-energy electron excitations in **4a** (red) and **4a^{•-}** (blue) as predicted by TD-DFT. Also shown are isosurfaces of the electron density differences ($\Delta\rho$) for each excitation with considerable oscillator strength. $\Delta\rho$ visualizes spatial distribution of the electron (yellow) and the hole (violet) in the exciton.

other MOs. TD-DFT calculations show that electron excitations of the radical anion **4a^{•-}** have more complex nature and cannot be well described by single configurations. The lowest energy transition has the main contribution (70%) from the HOMO \rightarrow SOMO excitation. Thus, it formally resembles the HOMO \rightarrow LUMO excitation of the neutral molecule, but comparison of $\Delta\rho$ isosurfaces shows that there is a considerable difference between them. Intensity and the energy of the transition in the radical anion are reduced dramatically. Presumably, this transition corresponds to the low-intensity absorption at 780 nm in the experimental spectrum. At higher energy, TD-DFT predicts two excitations near 545 nm (Figure 9), which presumably correspond to the strong band at 542 nm in the experimental spectrum (Figure 3a). In terms of MO configurations, both transitions have strongly mixed character. About 50% in each correspond to excitations from the SOMO to higher energy unoccupied MOs.

Calculations for **4b** give very similar results with small shifts of the excitation energies (see SI).

3. Conclusions

The results of electrochemical and spectroelectrochemical measurements at two differently chloro-substituted 4-(thiazol-2-ylazo)**4a** and **4b** demonstrate the rather high stability of the radical anions **4a^{•-}** and **4b^{•-}** and of the dianion **4a²⁻** as well as the low stability of the dianion **4b²⁻**. Moreover, quantum chemical calculations performed reproduce not only satisfactorily the optical properties of the radical anions **4a^{•-}** and **4b^{•-}**, but reveal also high hole densities in the LUMO of the neutral compounds **4a** and **4b** at the C1 and C4 positions in their naphthalene moieties and at the C5 position in their thiazole moieties which are responsible for the documented reactivity of these positions towards nucleophiles.^[6] Furthermore, the quantum chemical calculations indicate in the SOMO of the radical

anion **4b**^{•-} a high spin density at C5 in the thiazole moiety, which is similar to the spin density at C1 and C3 in the 1-chloronaphthalene moiety. Therefore, this thiazole C5 position seems suited for an alternative chloride elimination followed by a protonation at this position giving rise to the formation of the radical species **C** according to a mechanistic route depicted in Scheme 3, route 3. However, according to the calculated data, this position is not more favoured for a chloride elimination than the C1 and C3 positions in the naphthalene moiety, but it is sterically lesser protected by adjacent groups as in the naphthalene moiety.

Experimental Section

Cyclic voltammograms (CV) of the compounds **4a** and **4b** were carried out in acetonitrile containing 0.1 mol tetra-(*n*-butyl)hexafluorophosphate (*n*-Bu₄NPF₆) as supporting electrolyte using a one-compartment electrochemical cell with a platinum wire as working electrode, a platinum sheet as counter electrode and a silver chloride coated silver wire as pseudo reference electrode. All electrochemical measurements were performed under inert nitrogen atmosphere. All potentials were measured against the half-wave oxidation potential of ferrocene (Fc) in the same solvent.

In situ ESR/UV-Vis-NIR spectroelectrochemical experiments were performed in the optical ESR cavity (ER 4104OR, Bruker, Germany). ESR spectra were recorded by the EMXmicro X-band CW spectrometer (Bruker, Germany) at 100 kHz modulation. UV-Vis-NIR spectra were measured by the Avantes spectrometer AvaSpec-2048x14-USB2 with the CCD detector and AvaSpec-NIR256-2.2 with the InGaAs detector applying the AvaSpec software. Both the ESR spectrometer and the UV-vis-NIR spectrometer are linked to a HEKA potentiostat PG 390 (HEKA Elektronik, Germany), which triggers both spectrometers. Triggering is performed by the software package PotMaster v2x80. For the spectroelectrochemical experiments a flat cell was used. A laminated gold- μ -mesh (Goodfellow) as the working electrode, a silver chloride coated silver wire as the pseudo reference electrode, and a platinum wire as the counter electrode were used. The ESR and UV-Vis-NIR spectra were collected at a continuous potential scan rate (0.004 V/s, a rate allowing successive ESR spectra to be collected). Each UV-Vis-NIR spectrum was collected relative to that of the non-charged compound at the initial potential.

All DFT calculations were performed with the Orca package.^[11] Molecular structures of the studied compounds were optimized at the B3LYP-D3BJ/def2-TZVPP level, where D3BJ stands for dispersion correction. Solvation correction was taken into account using conductor-like polarizable continuum C-PCM model.^[12] In calcula-

tion of the hyperfine coupling constants basis sets for N and H atoms were replaced with the specially tailored EPR-III basis set.

Acknowledgements

The authors thank Sandra Schiemenz (IFW Dresden) for the measurements of the UV-Vis absorption spectra. Open access funding enabled and organized by Projekt DEAL.

Conflict of Interest

The authors declare no conflict of interest.

Keywords: azo compounds · spectroelectrochemistry · radical Anions · spin densities · DFT calculations

- [1] a) J. Casado, I. Gallardo, M. Moreno, *J. Electroanal. Chem.* **1987**, *219*, 197–208; b) R. A. Rossi, A. B. Pierini, A. B. Penenory, *Chem. Rev.* **2003**, *103*, 71–167.
- [2] A. Kuhn, K. G. von Eschwege, J. Conradi, *J. Phys. Org. Chem.* **2012**, *25*, 58–68.
- [3] A. B. Pierini, D. M. A. Vera, *J. Org. Chem.* **2003**, *68*, 9191–9199.
- [4] a) V. Kalyanarman, S. S. Dua, C. N. R. Rao, M. V. Gorge, *Tetrahedron Lett.* **1968**, *9*, 235–238; b) G. H. Aylward, J. L. Garnett, J. H. Sharp, *Chem. Commun.* **1966**, 137–138.
- [5] a) R. Podsiadly, J. Sokolowska, A. Marcinek, J. Zielonka, A. Socha, M. Kazmierska, *J. Photochem. Photobiol. A* **2005**, *171 A*, 69–76; b) Z.-U. Bae, H.-L. Lee, M.-L. Seo, *Bull. Korean Chem. Soc.* **1989**, *10*, 258–26.
- [6] X. Yu, P. Metz, H. Hartmann, *Eur. J. Org. Chem.* **2019**, 1317–1329.
- [7] S. Jasimuddin, D. G. Thaurata, *Trans. Met. Chem.* **2009**, *34*, 937–942; A. Kawase, *Bunseki Kagaku* **1963**, *12*, 709–714.
- [8] a) R. Günter, E. Jähne, H. Hartmann, M. Schulze, *J. Prakt. Chem.* **1987**, *329*, 945–954; b) M. Schulze, H. Hartmann, E. Berthold, DD 287724 **1991**; c) M. Schulze, H. Hartmann, E. Berthold, DD 288166 **1991**; d) H. Hartmann, E. Jähne, J. Liebscher, DD 155986 **1982**.
- [9] a) V. Kalyanarman, S. S. Dua, C. N. R. Rao, M. V. Gorge, *Tetrahedron Lett.* **1968**, *9*, 235–238; b) G. H. Aylward, J. L. Garnett, J. H. Sharp, *Chem. Commun.* **1966**, 137–138.
- [10] S. Stoll, A. Schweiger, *J. Magn. Reson.* **2006**, *178*, 42–55.
- [11] F. Neese, *WIREs Comput. Mol. Sci.* **2012**, *2*, 73–78.
- [12] M. Cossi, N. Rega, G. Scalmani, V. Barone, *J. Comput. Chem.* **2003**, *24*, 669–681.

Manuscript received: January 22, 2020

Revised manuscript received: March 19, 2020

Accepted manuscript online: March 19, 2020